Physicochemical characterization of clove essential oil-chitosan nanoparticles and resulting pectin films: Evaluation of the antimicrobial activity against *Pectobacterium carotovorum subsp. carotovorum*

Sondos Hejazi[1,2,3], Marika Avitabile[1], Mohammed Sabbah[3], Alessandro Polito[4], Valeria Scala[4], Angela Marotta[5], Ana Aleksov[6], C. Valeria L. Giosafatto[1]✉

[1] Department of Chemical Sciences, University of Naples "Federico II", Complesso Universitario di Monte Sant'Angelo, 80126 Naples, Italy
[2] Dipartimento di Agraria, University of Naples "Federico II", Parco Gussone, I-80055 Portici, Italy
[3] Department of Nutrition and Food Technology, An-Najah National University, Nablus P400, Palestine
[4] Research Centre for Plant Protection and Certification, Council for Agricultural Research and Economics (CREA-DC), Rome, Italy
[5] Department of Chemical, Materials and Production Engineering, University of Naples "Federico II", P.le Tecchio 80, 80125 Naples, Italy
[6] University of Novi Sad, Department of Chemistry, Biochemistry and Environment al protection at the Faculty of Science

Abstract

This study developed and characterized bio-based active packaging materials using pectin (PEC) films enriched with clove essential oil (CEO)-loaded chitosan nanoparticles (CHNPs). CEO was encapsulated within CHNPs via an emulsion ionic gelation technique, with varying concentrations investigated. The extracted CEO exhibited potent antioxidant activity (IC50 of 2.7 ± 0.13 µg/mL). Optimal encapsulation efficiency reached 16% (0.04 g CEO), and maximum loading capacity was 8% (0.16 g CEO). CHNPs averaged 200 nm with zeta potential up to +27 mV. These CEO-CHNPs were then incorporated into PEC films via polyelectrolyte complexation. Physicochemical characterization showed that integrating CEO-CHNPs into the PEC matrix enhanced the films' mechanical and thermal properties and improved their stability. Crucially, the in vitro antibacterial activity against *Pectobacterium carotovorum* subsp. *carotovorum* (Pcc), a significant post-harvest phytopathogen, was rigorously assessed. All tested formulations exhibited inhibitory activity against Pcc. Notably, CEO-CHNPs (0.16 g CEO initial load) at 0.3% (w/v) achieved total inhibition of Pcc growth at both 1- and 2-days post-inoculation. While some formulations showed decreased inhibition over time, the CHNPs+0.16 CEO formulation consistently demonstrated strong inhibitory capacity even at its lowest tested concentration (0.003% w/v). This enhanced potency is attributed to the synergistic action of CHNPs and CEO. These findings suggest CEO-CHNPs/PEC films are promising for extending food shelf-life, contributing to sustainable active packaging solutions.

Keywords: Chitosan nanoparticles. Clove oil encapsulation. Edible films. Enhanced film properties antimicrobial activity. Post-harvest spoilage

✉ Valeria Giosafatto
[1] giosafat@unina.it.
Department of Chemical Sciences, University of Naples "Federico II", 80126 Naples, Italy.

1. Introduction

Active packaging technologies are gaining prominence in the food industry due to their potential to extend shelf life, enhance safety, and maintain the quality of food products (Sabbah et al., 2023; Al-Asmar et al.,2020; Mirpoor et al., 2024; Corrado et al., 2021). A relevant example of this approach is the bioactive packaging developed by Abdalrazeq et al. (2021) from whey proteins and essential oil extracted from the Palestinian wild plant Thymbra (*Satureja capitata, L.*) (Abdalrazeq et al., 2021). Their research demonstrated that the addition of this essential oil significantly improved the films' antimicrobial activity against the foodborne bacteria *Enterococcus faecalis* and *Salmonella enterica* in a dose-dependent manner (Abdalrazeq et al., 2021; Arciello et al., 2021).

Beyond proteins, polysaccharides are also prominent bio-based materials gaining attention for active packaging. Pectin (PEC), an anionic polysaccharide primarily derived from Citrus fruits (e.g., *Citrus sinensis*), is widely used in the food industry due to its film-forming and gelling properties, often demonstrating favorable mechanical and barrier characteristics comparable to commercial plastics (Iijima et al.,2000; Giosafatto et al., 2014). To further enhance these properties and incorporate active functionalities, chitosan (CH), a linear cationic polysaccharide from crustacean shells, can be employed. CH's positive charge allows it to interact with PEC's negative charge through polyelectrolyte complexation, resulting in improved film properties (Hosseiniet al., 2023).

Additionally, CH can be formed into nanoparticles (CHNPs), which offer advantages such as biocompatibility, biodegradability, and non-toxicity (Hu et al., 2016; Younes et al., 2015). CHNPs are excellent carriers for active ingredients like clove essential oil (CEO), extracted from the buds of *Syzygium* aromaticum. This aromatic plant, cultivated in tropical and subtropical countries, is rich in bioactive compounds including eugenol, eugenyl acetate, and β-caryophyllene (Hasheminejad et al., 2019; Chaieb et al., 2007; Sebaaly et al., 2015). These compounds imbue CEO with potent antimicrobial and antioxidant properties, making it valuable for extending food shelf life and inhibiting spoilage (Hasheminejad et al., 2019; Chaieb et al., 2007; Sebaaly et al., 2015; Jamil et al., 2016). However, the direct application of CEO is limited by the volatile and slightly water-soluble nature of its components (Woranuch et al., 2013; Katouzian et al., 2016). Encapsulation of CEO within CHNPs offers an effective strategy to overcome these limitations and facilitate its incorporation into edible films (Giosafatto et al., 2014). The ion gelation process, particularly the emulsion-ionic gelation technique, is a straightforward method that utilizes tripolyphosphate (TPP) as a crosslinker to form CHNPs. This technique is well-suited for enhancing active compound stability, preserving their beneficial properties, and controlling their release profile (Hejazi et al., 2023a, 2024b)

While active packaging offers broad benefits, a critical challenge in extending the shelf life of fresh produce is the control of post-harvest phytopathogens. Among these, *Pectobacterium carotovorum* subsp. *carotovorum* (Pcc) poses a significant threat. This Gram-negative bacterium causes destructive soft rot, wilt, and black leg in various crops by producing enzymes that degrade plant cell walls (Lim et al., 2013). The widespread distribution and severe pathogenicity of Pcc underscore an urgent need for effective antimicrobial strategies to safeguard food products post-harvest.

In this study, we employed ion gelation to encapsulate clove essential oil (CEO) within chitosan nanoparticles (CHNPs), which were then incorporated into pectin (PEC) films via polyelectrolyte complexation, as described by Hejazi et al. 2023a, 2024b. We comprehensively characterized the resulting CEO-CHNPs/PEC films, evaluating their physicochemical properties (including CEO antioxidant activity, encapsulation efficiency, and loading capacity), mechanical and thermal properties, morphology, and water vapor permeability. Importantly, we also assessed the antibacterial activity of these films against the significant post-harvest phytopathogen, *Pectobacterium carotovorum* subsp. *carotovorum* (Pcc). This research aims to provide a comprehensive understanding of the properties of CEO-CHNPs/PEC films, contributing to the development of novel bio-based active packaging materials for enhanced food preservation.

✉ Valeria Giosafatto
[1] giosafat@unina.it.
Department of Chemical Sciences, University of Naples "Federico II", 80126 Naples, Italy.

2. Materials and methods

Materials

PEC from *Citrus* peels (galacturonic acid content 93.5%; methoxyl content 9.4%; dry matter 55.3%; pKa=3.0–4.5), CH (75–85% deacetylated chitin, poly-D-glucosamine, 50–190kDa), glycerol (GLY), sodium tripolyphosphate (STPP), Tween 80, and 2,2-diphenyl-1-picrylhydrazyl (DPPH) were purchased by Sigma Aldrich, St. Louis, MO, USA); clove pods were from a local market in Naples, Italy, n-hexane was purchased from Carlo Erba Reagents (Val de Reuil, France).

2.1. Clove essential oil (CEO) extraction and antioxidant activity evaluation

Clove flower buds were crushed using a Knife Mill (Retsch GmbH, Haan, Retsch-Allee, Germany) to extract clove oil using the Soxhlet apparatus for oil extraction through distillation as described by Mirpoor et al., 2022 with some modifications. Approximately 25 g of clove buds were ground for oil extraction using n-hexane distillation. The resulting powder was placed into a filter paper extraction thimble, which was then inserted into the lower part of the Soxhlet extractor. A flask containing 200 mL of n-hexane was positioned below, and the system was heated to a temperature of 100ºC. The Soxhlet column was connected to a reflux condenser, and the entire setup was heated on a mantle until n-hexane began to boil. During the process, the boiling vapor ascended through the condenser, condensed, and fell back onto the porous thimble containing the powdered sample. This mixture was collected in the receiver of the Soxhlet extractor setup over 6 hours. Subsequently, the extracted oil was concentrated using a rotary evaporator (STRIKE 300, Steroglass S.r.l -Perugia, Italy), and the CEO yield was calculated as follows:

$$\%Yield\ of\ essential\ oil = \left[\frac{Essential\ oil\ weight\ (g)}{Sample\ weight\ (g)} \times 100\right] \quad (1)$$

The antioxidant activity of CEO was evaluated using the technique of radical scavenging capacity with 1,1-diphenyl-2-picrylhydrazyl (DPPH) radical according to the method of Lesjak et al., 2018. Ten microliters of each sample, with initial concentrations of CEO from 0.01 to 10 mg/mL were combined with 100 µL of 67.5 µmol/L DPPH solution in methanol. The resulting mixture was then diluted with an additional 190 µL of methanol. In the control group, 10 µL of the sample was replaced with distilled water. For blank probes, 290 µL of methanol was mixed with each sample (10 µL), while the blank probe for the control involved the addition of only 300 µL of methanol. Absorbance measurements were taken at 515 nm after 1 hour using a microplate reader (Benchmark Plus, BIO-RAD Laboratories, Inc, Italy), and all samples and controls were prepared in triplicate. The antioxidant potential of each sample concentration was determined by calculating the percentage of inhibition using the formula (2) where the absorbance was corrected for the corresponding blank probe values.

$$\%\ Inhibition = \left[\frac{Absorbance\ of\ the\ control - Absorbance\ of\ the\ sample}{Absorbance\ of\ the\ control} \times 100\right] \quad (2)$$

Inhibition-concentration curves were constructed using OriginLab software, version 2023b for Windows with the Growth/ Sigmoidal function category (Roundhouse Plaza, Northampton, MA, USA), and IC_{50} values (the concentration of the extract inhibiting DPPH radical formation by 50%) were determined. The results for each assay were expressed as the mean ± standard deviation (SD) based on three measurements.

2.2. Clove essential oil (CEO) encapsulation

Oil-loaded and unloaded particles were prepared in two steps: droplet formation and solidification, adapting the methodology of Hosseini et al., 2019. First, CH solution (1% w/v) was dissolved in 1% (v/v) acetic acid solution by stirring overnight at 25°C. The pH was then adjusted to 4.6 with 0.5 N NaOH, and 0.45 g of Tween 80 (HLB 15.9) was added as an emulsifier to 40 mL of the CH solution. After stirring at 45°C for 2 hours, the desired amount of CEO (0.04, 0.16, or 0.32 g) was dissolved in 4 mL of CH_2Cl_2 and gradually dropped to the aqueous CH solution. The mixture was then agitated at 700 rpm for 10 minutes at 25°C in an ice bath using an Ultra-Turrax T25 basic (IKA, Germany) to create an oil-in-water emulsion. Next, 40 mL of 0.4% (w/v) STPP solution was prepared in distilled water and added to the emulsion. The mixture was agitated for 30 minutes to facilitate

crosslinking, and the final pH was adjusted to 4.6. Unloaded particles were prepared using the same procedure, omitting the addition of CEO. The resulting CEO-CHNPs were collected by centrifugation (Avanti J-20 XP, Beckman Coulter, Brea, CA, USA) at 9000×g for 30 minutes at 4°C, washed multiple times with a 1% (v/v) aqueous Tween 80 solution, and then dispersed in distilled water. The dispersion was sonicated for 10 minutes using a Bandelin SONOPULS ultrasonic homogenizer (Binder, Tuttlingen, Germany) with a sequence of 3 seconds sonication and 7 seconds rest. The homogenized dispersions were stored at 4°C until further analysis. A portion of the prepared dispersions was freeze-dried at −40°C for 24 hours (Thermo Savant Modulyo Benchtop, USA).

2.3. Encapsulation efficiency (EE), loading capacity (LC) and yield determination

To assess the effectiveness of the encapsulation process, the loading capacity (LC) and encapsulation efficiency (EE) of CEO in CHNPs were analyzed using UV-vis spectroscopy-(SmartSpec™ 3000, Bio-Rad Laboratories, Inc - Italy). A 1:1 (w/w) ratio of CH to STPP was used for the preparation of CHNPs. The methodology followed the procedures outlined by Rahaiee et al., 2015; Feyzioglu and Tornuk, 2016 with some modifications. For the determination of CEO encapsulation, 10 mg/mL CEO-CHNPs were mixed with an aqueous hydrochloric acid solution (2M, 5 mL) and boiled at 95°C for 30 min. After cooling, 1 mL of ethanol was added, and the mixture was centrifuged. Blank CHNPs were also prepared using the same method. CEO loading was determined by UV-vis spectroscopy at 282 nm using a standard curve. The measurements were conducted in triplicate. Encapsulation efficiency (EE), loading capacity (LC) and yields were calculated using the following formulas:

$$\% EE = \left\lfloor \frac{Total\ weight\ of\ loaded\ CEO}{Initial\ weight\ of\ CEO} \times 100 \right\rfloor \quad (3)$$

$$\% LC = \left\lfloor \frac{Total\ weight\ of\ loaded\ CEO}{Weight\ of\ freeze\ dried\ NPs} \times 100 \right\rfloor \quad (4)$$

$$\% CHPs\ Yield = \left\lfloor \frac{Weight\ of\ freeze\ dried\ NPs}{Sum\ of\ the\ dry\ weights\ of\ initial\ materials} \times 100 \right\rfloor \quad (5)$$

2.4. Fourier Transform Infrared Spectroscopy Analysis (FTIR)

Spectra were recorded by an FTIR instrument (JASCO FT/IR-4700, JASCO EUROPE S.R.L., Italy), and 64 scans interferogram was collected with a variable path length cell and KBr windows. Samples were combined with dry KBr. The grounded mixture was then pressed into a transparent desk. The spectra were recorded at a straight baseline of 400–4000 cm^{-1}.

2.5. Pectin-based films prepared with clove essential oil-chitosan encapsulated nanoparticles (CEO-CHNPs/PEC)

Pectin-based films were prepared by incorporating CEO-CHNPs. *Citrus* pectin (PEC) was used to prepare a 2% (w/v) stock solution. A 40 mL aliquot of this solution was mixed with 30% GLY (w/v, relative to PEC) as a plasticizer, and the pH was adjusted to 7.2 using 0.1N NaOH. Three experimental groups were prepared, each containing 5 mg of freeze-dried CEO-CHNPs (prepared at CH to CEO mass ratios of 1:0.1, 1:0.4, and 1:0.8) dissolved in 10 mL of 1% acetic acid and blended with the PEC solution using a polyelectrolyte complexation approach Hejazi et al., 2023a, 2024b. Two control groups were also prepared: one containing 5 mg of freeze-dried CHNPs without CEO, dissolved in 10 mL of 1% acetic acid and added to the PEC solution, and another consisting of a pure PEC film (40 mL PEC with 30% GLY mixed with 10 mL distilled water). The resulting film-forming solutions (FFSs) were cast onto leveled 8 cm diameter polystyrene Petri dishes and dried at 25°C and 50% relative humidity for 48 hours. The dried films were then conditioned in a desiccator at 25 °C and 50-55% RH using a saturated $Mg(NO_3)_2.6H_2O$ before analysis. This resulted in the formation of a homogeneous and handleable PEC film containing CEO-CHNPs. These films were named as follows: 0 CEO-CHNPs/PEC, 0.1 CEO-CHNPs/PEC, 0.4 CEO-CHNPs/PEC, and 0.8 CEO-CHNPs/PEC, corresponding to the following ratios between CH to CEO: 1:0.0, 1:0.1, 1:0.4, and 1:0.8 (where PEC stands for 800 mg of pectin).

2.6. *In vitro* evaluation of antibacterial activity against *Pectobacterium carotovorum* subsp. *carotovorum* (Pcc)

CEO,CH, CHNPs and CEO-CHNPs (CHNPs+0.04CEO, CHNPs+0.16CEO, CHNPs+0.32CEO) were tested to evaluate the bacterial growth (BG) inhibition of Pcc. The substances were tested at 0.3%, 0.03% and 0.003% (w/v or v/v only for CEO) dilutions. All the substances are soluble in water, only CEO was dissolved in dimethyl sulfoxide (DMSO): 40 µL of CEO were added to 525 µL DMSO. Each substance at different concentrations was tested in three replicate wells containing bacteria and three wells without bacteria. Each well was filled with 180 µL of the test substance and 20 µL of either the bacterial suspension in nutrient broth (NB) (OD_{600}= 0.01) or sterile NB for the blanks. Additionally, three wells with bacteria in NB and three with sterile NB were prepared as positive and negative controls respectively. For CEO, dissolved in DMSO, references with a corresponding concentration of DMSO but without the compound were used as background. The microplate was incubated at 26 °C at 100 rpm and the bacterial growth was evaluated measuring OD_{600} after 1- and 2-day post inoculation (dpi). The experiment was repeated twice. CREA-DC 1241 Pcc strain was selected from the collection of Research Centre for Plant Protection and Certification, Council for Agricultural Research, and the Analysis of Agricultural Economics (CREA-DC). The strain was freeze-dried for preservation and grown on Nutrient Agar 0.25% d-glucose (NAG) for three days at 26 °C before proceeding with *in vitro* analysis. After three days the bacteria were collected from NAG plates and suspended in NB and the optical density were adjusted to OD_{600}= 0.01.
Statistical analysis was carried out using GraphPad Prism 8 Software (GraphPad Software, San Diego, CA, USA). Differences between the control and treated samples were evaluated using one-way ANOVA and means were separated by Tukey's test, with statistical significance defined as $P < 0.05$.

2.7. Film forming solution (FFS) and film characterization

2.7.1. Size and zeta potential

A Zetasizer Nano-ZSP (Malvern®, Worcestershire, UK) was employed to determine the size and zeta potential of both FFS and CHNPs. Three independent measurements were carried out on each sample (0.5 mg/mL).

2.7.2. Mechanical properties

Evaluation of film mechanical behavior including Young's modulus (YM) tensile strength (TS) and elongation at break (EB) was performed using an Instron 5543A instrument (Instron Engineering Corp., Norwod, MA, USA) following the instructions of ASTM standard D882-97.

2.7.3. Water vapor permeability (WVP)

WVP of the film was assessed using a MultiPerm apparatus (ExtraSolution s.r.l, Pisa, Italy) following the standard method ASTM F1249-13. The WVP permeability was measured at 50% RH, 25°C, and 1.585 kPa. Before testing, the films underwent a 24-hour conditioning period at 50% RH and were enclosed in aluminum masks to decrease the film test area to 2 cm^2.

2.8. Thermal analysis

Thermal characteristics of freeze-dried CHNPs and PEC-based films were determined by thermogravimetric analysis (TGA) and differential scanning calorimetry (DSC). TGA was conducted with a TA Q50 (TA Instrument, New Castle, DE, USA) in an oxidative atmosphere (air, 600ml/min), heating the samples at 10°C/min up to 600°C. DSC was performed with a TA Q2000 (New Castle, DE, USA) equipped with a refrigerator cooling system (RCS), heating the samples from -50°C to 150°C at a 10°C/min heating rate.

2.9. Statistical analysis

The results are expressed as mean ± standard deviations from three replicates. Statistical analyses were conducted using Microsoft Excel software (Microsoft Office 2017). The data underwent t-test analysis, and significance was attributed to values with $p<0.05$.

3. Results and Discussion

3.1. Clove essential oil (CEO) yield

The final yield of CEO obtained was 18% ± 1. This yield is comparable to previously reported values of 19.5% obtained using supercritical fluid extraction (Guan et al., 2007). However, the Soxhlet extraction method, known for its milder conditions, is expected to favor the extraction of volatile compounds like eugenol, the primary component of CEO. It is worth noting that the particle size of the starting material can influence extraction yield, with smaller particles generally leading to higher yields due to increased surface area (Khajehet al., 2004; Reverchon 1997). However, a balance must be struck between maximizing extraction yield and preserving the desired composition of the CEO.

3.2. Clove essential oil antioxidant activity

The effectiveness of antioxidants is often measured by IC_{50}, which is the concentration needed to neutralize 50% of free radicals. Lower values indicate stronger antioxidant activity. In this study, CEO's antioxidant potential against DPPH radicals was evaluated at various concentrations (0.002 - 2.5 mg/mL). **Fig. 1** shows a graph depicting the scavenging capability (ability to neutralize free radicals) increasing with concentration. Notably, CEO exhibited a potent scavenging ability with an IC_{50} of 2.7 ± 0.13 µg/mL obtained by DPPH, indicating its effective antioxidant potential. The robust antioxidant efficacy of CEO may be attributed to its high phenolic content, notably eugenol, which serves as a protective agent against damage induced by reactive oxygen species (Kiki et al., 2023). This aligns with findings from Selles et al. 2020 who reported an IC_{50} value of 4.82 ± 0.06 × 10^{-2} µg/mL for the antioxidant activity of the same CEO by means of the DPPH assay.

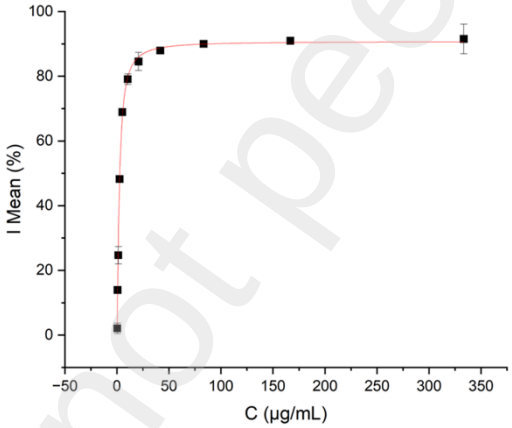

Fig. 1. Dependence of inhibition (I mean %) on working concentration (C, µg/mL) of the clove essential oil (CEO) as investigated by DPPH free-radical-scavenging activity of CEO.

3.3. Encapsulation efficiency (EE), loading capacity (LC), and yield

Table 1 presents the yield percentage of the encapsulated particles, with the loading of CEO into CHNPs decreasing as the amount of CEO increased, consistent with findings from Hosseini et al. 2023 EE ranged from 3% to 16%, with the highest EE (16%) at CEO content of 0.04 g. Maximum EE was achieved at a CH to CEO weight ratio of 1:0.1. LC ranged from 8% to 3% with varying CEO content. The decline in EE at higher CEO concentrations is likely due to the saturation of CEO in CHNPs, as supported by previous research (Hasheminejad et al., 2019; Ajunet al., 2009; Yoksanet al., 2010).

3.4. *In vitro* evaluation of antibacterial activity against *Pectobacterium carotovorum* subsp. *carotovorum* (Pcc)

As can be seen in Fig. 2 and 3, all tested products showed inhibitory activity against Pcc. In fact, all of them show statistically significant differences compared to their respective controls, except for CEO 0.003% v/v which shows the same BG as its control in DMSO (Fig 2a, 3a) and for Chitosan 0.003% w/v (Fig. 2b) and CHNPs+0.04CEO 0.003% w/v (Fig. 2d) after 1 dpi. In many of the theses, BG values increased after two days and inhibition decreased at 2 dpi. This is probably due to degradation of the inhibitor molecules, but further investigations are needed. In Fig. 2a, 2c, 2e, 3a, 3c and 3e it's possible to see that the most effective theses were CEO, CHNPs and CHNPs+0.16CEO at the highest concentration (0.3%) both 1 and 2 dpi, which showed total inhibition of BG. CEO 0.03% v/v showed very high inhibition, reducing BG by approximately half compared to the DMSO control 0.03% v/v at both 1 and 2 dpi (Fig. 2a, 3a). Chitosan 0.3% w/v also caused a reduction in BG compared to the NB control at 1 dpi, but its activity appeared to have decreased at 2 dpi (Fig 2b, 3b). Chitosan 0.03% w/v showed a BG OD_{600} of 0.26 at 1 dpi and 0.37 at 2 dpi, also demonstrating a good inhibitory capacity related to NB control which had a BG OD_{600} respectively of 0.4 and 0.46 (Fig. 2b, 3b). Chitosan 0.003% w/v at 2 dpi achieved a similar result to Chitosan 0.03% w/v (Fig. 3b). CHNPs 0.03 and 0.003% w/v had similar inhibition as Chitosan 0.03% w/v at 1 dpi, but at 2 dpi reduced their activity (Fig. 2c, 3c). As for the CHNPs+0.04CEO thesis, the concentrations that achieved performances like Chitosan 0.03% w/v were 0.3 and 0.03% w/v at 1 dpi and 0.3 and 0.003% w/v at 2 dpi (Fig. 2d, 3d). CHNPs+0.04CEO 0.03% w/v reduced its activity at 2 dpi, but there are no statistically significant differences compared to CHNPs+0.04CEO 0.003% w/v (Fig. 3d). CHNPs+0.16CEO 0.03% w/v had a good inhibition at 1 dpi showing a BG OD_{600} of 0.27 and at 2 dpi approximately halved the BG compared to NB control (Fig. 2e, 3e). CHNPs+0.16CEO 0.003% w/v showed a BG OD_{600} of 0.27 at 1 dpi and 0.33 at 2 dpi, demonstrating a good inhibitory capacity also at the lowest concentration (Fig. 2e, 3e). CHNPs+0.32CEO 0.3% w/v showed similar inhibition as Chitosan 0.03% w/v both at 1 and 2 dpi (Fig. 2f, 3f). CHNPs+0.32CEO 0.03% w/v demonstrated the same activity only at 2 dpi (Fig. 3f). At the lowest concentration CHNPs+0.32CEO had inhibition but very low (Fig. 2f, 3f). Analyzing these results, it is possible to mention the CHNPs+0.16CEO as a performing product, since its inhibition of BG it's good even at the lowest concentration tested both after one and two days from inoculation.

The antibacterial activity of CH, CHNPs, CHNPs+EOs, and CEO against Pcc was confirmed in this study, in line with previous research (Sotelo-Boyas *et al.*, 2015; Zhang *et al.*, 2023; Jilkova *et al.*, 2024). However, to the best of our knowledge, this is the first report demonstrating the antibacterial efficacy of the CHNPs+CEO combination specifically against Pcc. The results suggest that the simultaneous action of CHNPs and CEO enhances the antimicrobial effectiveness of the CHNPs+CEO formulation. This synergistic effect may be attributed to the unique properties of each component. Nanoparticles, due to their high surface area and ability to agglomerate on microbial membranes, increase contact with the cell wall and thus exhibit heightened reactivity (Sanpui *et al.*, 2008; Chen *et al.*, 2009; Radzig *et al.*, 2013). Meanwhile, CEO, particularly its main component eugenol, has been shown to inhibit the transcription of quorum sensing genes in bacteria, thereby reducing biofilm formation and the production of extracellular enzymes (Joshi *et al.*, 2016). Together, these mechanisms likely contribute to the increased antimicrobial potency observed in the CHNPs+0.16CEO treatment.

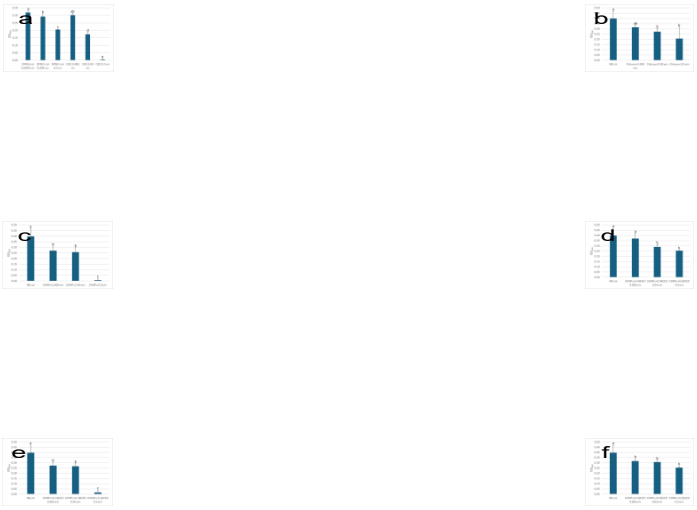

Fig. 2. Bacterial growth in *in vitro* test of *Pectobacterium carotovorum* subsp. *carotovorum* after 1 dpi. (a) comparison of effect of CEO thesis with DMSO controls; (b) comparison of effect of chitosan thesis with NB control; (c) comparison of effect of CHNPs thesis with NB control; (d) comparison of effect of CHNPs+0.04CEO thesis with NB control; (e) comparison of effect of CHNPs+0.16CEO thesis with NB control; (f) comparison of effect of CHNPs+0.32CEO thesis with NB control. Different letters on top of the bars indicate a significate difference between the treatments according to Tuckey test $P < 0.05$. Identical letters indicate a no significant difference between the treatments.

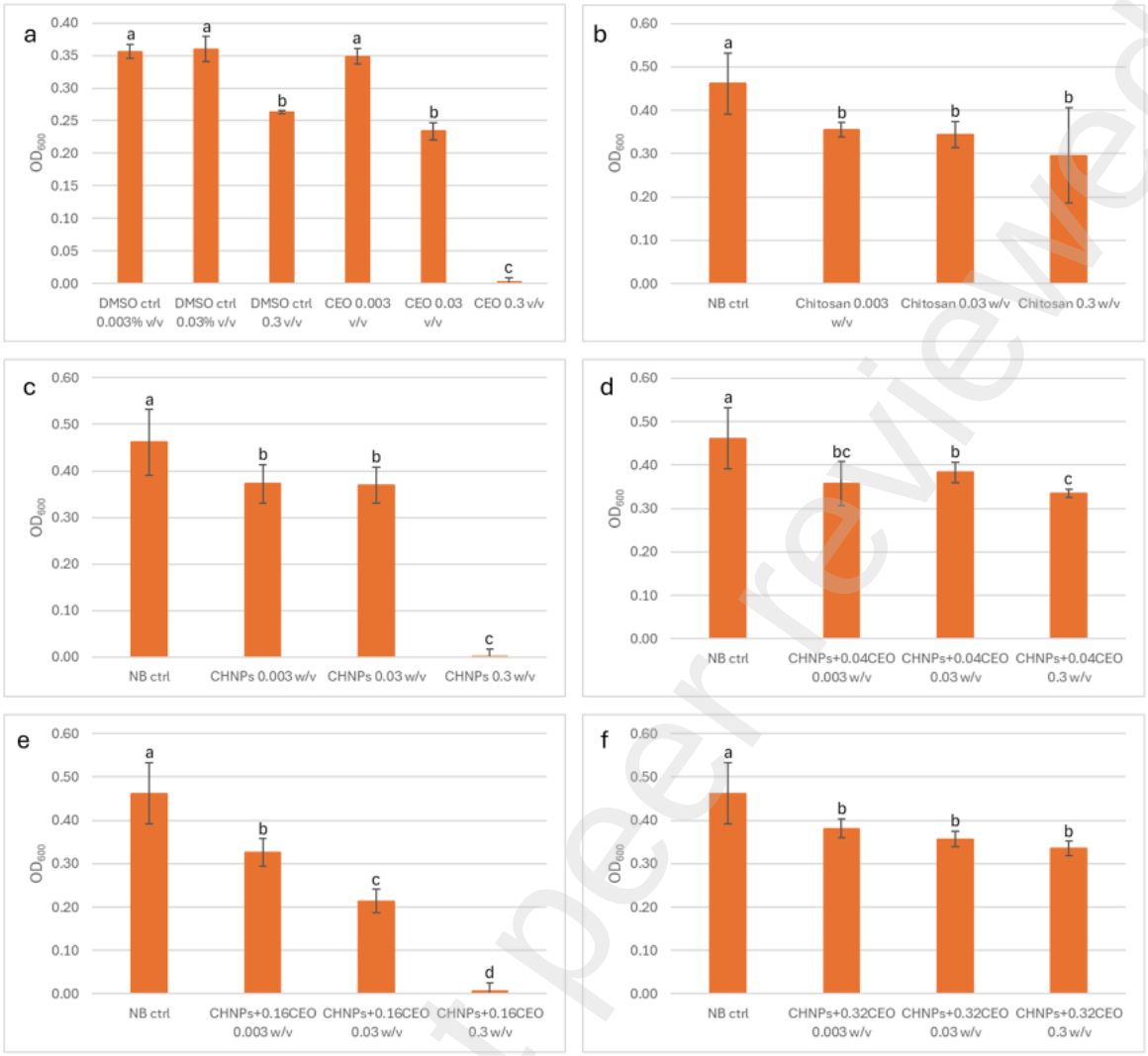

Fig. 3. Bacterial growth in *in vitro* test of *Pectobacterium carotovorum* subsp. *carotovorum* after 2 dpi. (a) comparison of effect of CEO thesis with DMSO controls; (b) comparison of effect of chitosan thesis with NB control; (c) comparison of effect of CHNPs thesis with NB control; (d) comparison of effect of CHNPs+0.04CEO thesis with NB control; (e) comparison of effect of CHNPs+0.16CEO thesis with NB control; (f) comparison of effect of CHNPs+0.32CEO thesis with NB control. Different letters on top of the bars indicate a significate difference between the treatments according to Tuckey test $P < 0.05$. Identical letters indicate no significant difference between the treatments.

3.5. Particle size and surface charge measurements of encapsulated particles

The impact of CEO addition on both size and surface charge, utilizing the ion gelation technique, was examined by means of a Zetasizer Nano, and is detailed in **Table 1**. Employing this method and introducing STTP led to a significant reduction in the average particle size. While it did not reach the typical nanoparticle range of 1-100 nm, the resulting particles are still considered polymeric nanoparticles (Rodríguez et al., 2016; He et., 2010). **Table 1** illustrates that untreated CH had an initial size of 1271 d.nm, while the addition of STPP reduced it to 353 d.nm. This size reduction may be attributed to enhanced polymer chain packing, facilitated by the abundant amino groups in CH that interact with the STPP (Russo et al., 2014). Furthermore, the influence of increasing CEO concentration on the average size and surface charge of CEO-loaded particles was investigated. In our study, the addition of varying amounts of oil resulted in decreasing average size, measuring 261 d.nm, 287 d.nm, and 212 d.nm for 0.04 g CEO, 0.16 g CEO, and 0.32 g CEO, respectively. Regarding surface charge, it was +67 mV for CH, decreasing significantly to +24 mV for the 1:0.0 CH: CEO ratio, and experiencing a slight increase with the highest CEO amounts, reaching +27 mV for the 1:0.8 CH: CEO ratio. Higher stability with a higher surface

charge might be attributed to the completion of ion crosslinking due to increased protonation of amino groups (**Table 1**) (Hasheminejad et al., 2019; Woranuch et al., 2013).

Table 1. Encapsulation efficiency (EE%) and loading capacity (LC%) of CEO in CH nanoparticles (CHNPs) determined by UV–vis spectrophotometry, and Z-average diameter and zeta potential of 0.5 mg/mL CHNPs loaded with CEO using dynamic light scattering.

CHNPs: CEO mass ratio (w/w)	%EE	%LC	Yield (%)	Z-average diameter (d.nm)	Zeta potential (mV)
1:0.0:0.0	0	0	-	1271±170	67±1
1:1:0.0	0	0	11.6±2	353±15 [a]	24±3 [a]
1:1:0.1	16±0.83	3±0.3	17.6±1 [b]	261±31 [a,b]	23±2 [a]
1:1:0.4	13±2.0	8±0.5	18.5±3 [b]	287±34 [a,b]	26±3 [a]
1:1:0.8	3.0±0.4 [c]	4±0.1 [c]	14.2±1 [b]	212±40 [a,b]	27±4 [a]

The values that are significantly different compared to CH indicated by "a" ($p < 0.05$); the values indicated by "b" are significantly different ($p < 0.05$) from CH unloaded with CEO; the values indicated by "c" are significantly different ($p < 0.05$) from 1:1:0.1 of CHNPs: STPP: CEO.

3.6. Fourier transform infrared (FTIR) characterization

The chemical structure of CH powder, CEO, CHNPs, and CEO-loaded CHNPs were characterized by FTIR as illustrated in **Fig. 2**. The spectrum of CH exhibited distinctive peaks, including those at 3439 cm^{-1} (O–H stretching), 2883 cm^{-1} (C–H stretching), 1659-1553 cm^{-1} (amide I stretching vibration), 1259 cm^{-1} (C-N stretching and bending vibrations), 1378 cm^{-1} (C–N stretching), 1157 cm^{-1} (β−(1–4) glycosidic linkage), and 1074 cm^{-1} (C–O–C stretching of glucose ring) (**Fig. 2a**) (Woranuch et al., 2013; Russo et al., 2014). The FTIR analysis identified characteristic peaks at 3439, 1659, 1550, 1324, 1594, 1422, and 1378 cm^{-1}, corresponding to N-H and O-H stretching vibrations, amide I and II, C-N stretching, and CH_2 and CH_3 deformations, respectively (Hejazi et al., 2023a; 2024b). In the context of CHNPs, a comparative analysis of the CH spectrum (**Fig. 2b**) reveals notable changes. Most peaks in the CHNPs spectrum are sharper, and a shift to the right is observed, indicative of interactions between the functional groups of CH and STPP. The emergence of a new peak at 2926 cm^{-1} in the FTIR spectrum of CH with STPP, in contrast to neat CH, suggests the presence of aliphatic C-H stretching vibrations. This new peak is likely indicative of alterations in the aliphatic C-H bonding resulting from the interaction between CH and STPP. Another new peak at 1740 cm^{-1} suggests that STPP may induce crosslinking reactions between CH molecules, potentially leading to the formation of new chemical bonds and the appearance of a carbonyl stretching peak. The interaction with STPP might also influence the degree of acetylation in CH, potentially resulting in the appearance of carbonyl groups. Moreover, specific changes in the FTIR spectrum include the shifting of the $N–H_2$ bending peak of amide II from 1553 to 1540 cm^{-1}. Additionally, new peaks at 1096 and 1250 cm^{-1} are observed, attributed to the stretching vibrations of PO_3 groups and P=O, respectively. These findings suggest complex formation through electrostatic interaction between the ammonium groups of CH and the phosphoric groups of STPP (**Fig. 2b**) (Sotelo-Boyás et al., 2017). The spectrum of pure CEO revealed numerous peaks corresponding to various volatile compounds, with notable peaks at 3525 cm^{-1} (O–H stretching), 2927–2850 cm^{-1} (C–H stretching), and 1603 and 1431 cm^{-1} (C=C stretching of the aromatic ring) (**Fig. 2f**) (Woranuch et al., 2013; Yoksan et al., 2010; Keawchaoonet al., 2011). Eugenol, a major component of CEO, exhibited characteristic peaks at 1511 cm^{-1} and 1614 cm^{-1}, corresponding to the C=C stretching of the aromatic moiety. Additional peaks observed at 1265, 1236, 915, 818, and 795 cm^{-1} were attributed to specific vibrational modes of eugenol and eugenol acetate (**Fig. 2f**). In the spectrum of CHNPs-CEO, where different amounts of CEO (0.04, 0.16, and 0.32 g) were encapsulated, peaks at 1731 cm^{-1} (related to CH spectrum) and several peaks at 1539, 1265, 953, and 850 cm^{-1} (related to CEO spectrum) were monitored (**Fig. 2c-e**). The increased intensity of peaks at 2926–2849 cm^{-1} (C–H stretching) and 1454 cm^{-1} (C=C stretching vibration of the aromatic ring) suggested potential interaction between CEO and CH matrix (**Fig. 2c-e**) (Woranuch et al., 2013; Yoksan et al., 2010; Keawchaoonet al., 2011). Notably, the spectra of CEO-loaded CHNPs (**Fig. 2 c-e**) exhibited a new and intense peak at 1652 cm^{-1}, indicating the successful encapsulation of CEO within CHNPs. The shifting of this

peak to the right with increasing CEO amount further supported successful encapsulation and suggested changes in the chemical environment (**Fig. 2c-e**).

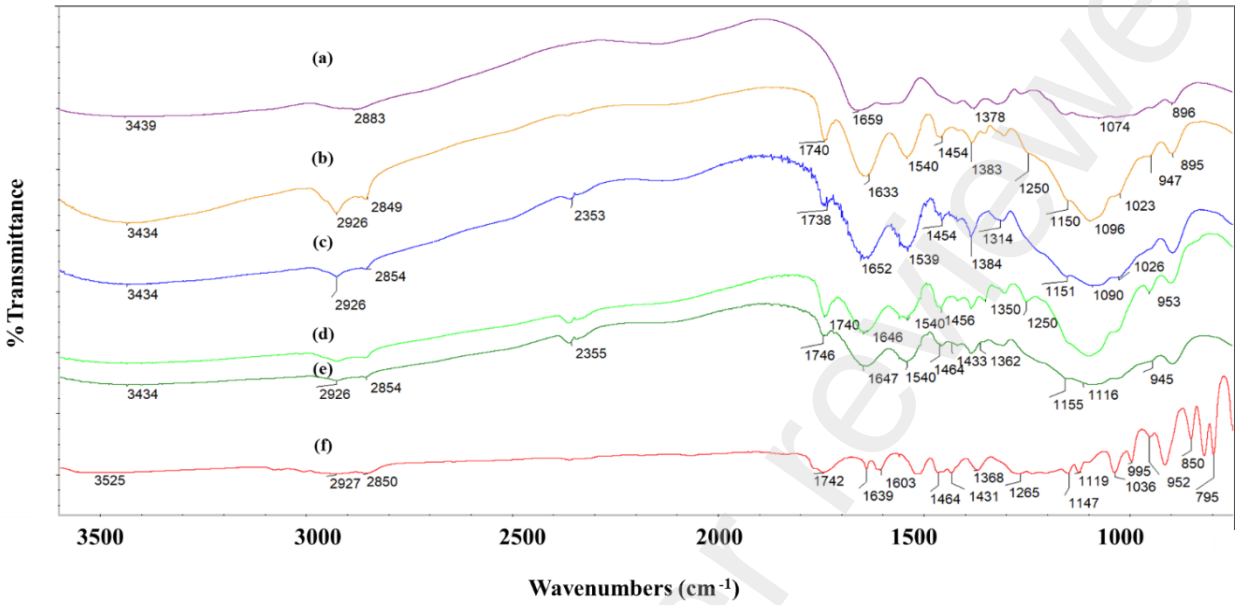

Fig. 2. FTIR spectra of (a) CH powder; (b) CH nanoparticles (CHNPs), (f) Clove Essential Oil (CEO), and CEO-loaded CHNPs (c-e). The CHNPs/CEO ratios examined include (c) 1:0.1; (d)1:0.4; (e) 1:0.8.

3.7. CEO-loaded CHNPs thermal stability

The thermograms from the DSC investigations are shown in **Fig. 3a**, where a large exothermic peak can be recognized for each sample. This is related to the loss of water during the dehydration of CH (Keawchaoon et al., 2011; Alkhader et al., 2017; De Mouraet al., 2008). When pristine CH is crosslinked to generate CHNPs, its dehydration temperature (T_D) rises from 77°C to 91°C. Furthermore, the total heat released during the dehydration process increases significantly, indicating a greater interaction between water and CH in the form of nanoparticles. The addition of the CEO to the CHNPs leads to a decrease in the T_D (about 83-85°C), in agreement with the CEO LC previously reported: the higher the CEO loading, the lower are T_D and the related reaction enthalpy. These results are in good agreement with the TGA analysis (**Fig. 3b**), where it can be noticed that the CH sample experienced a lower weight loss up to 100°C (i.e., loss of hydration water), compared to the CHNPs at the various loadings. The thermal stability of CHNPs decreases if compared to that of CH, as reflected by the decrease in degradation temperature from 300°C for CH to 242°C for the CHNPs. However, the nanoparticles show a higher thermal resistance at high temperatures (above 400°C), as also reflected by the presence of a residue at 600°C.

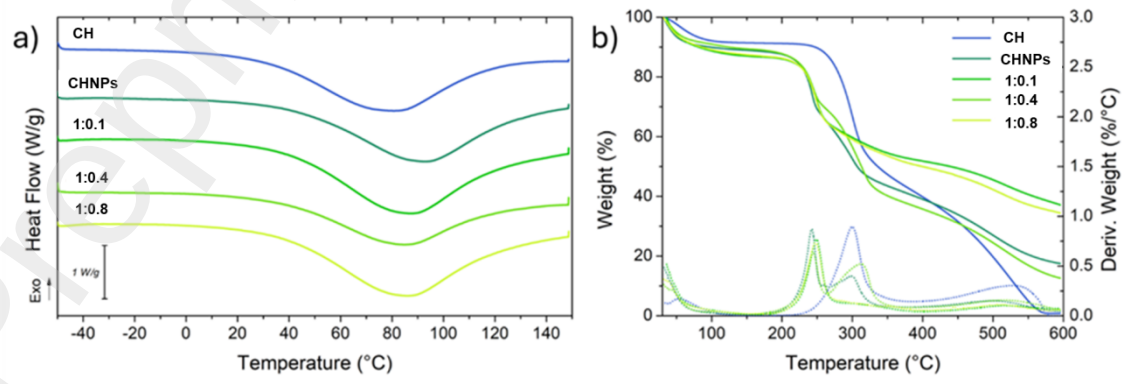

Fig. 3. (a) DSC and (b) TGA thermograms of CH powder, CH nanoparticles (CHNPs) and CEO-loaded CHNPs at different CHNPs/CEO ratios: 1:0.1, 1:0.4, 1:0.8.

3.8. Characterization of film forming solutions (FFSs) and the derived films

3.8.1. Particle size and surface charge measurements

Table 2 presents the average particle size, zeta potential and polydispersity index (PDI) of the FFS prepared with varying CEO concentrations. The average particle size of the FFSs increased with increasing CEO concentration, reaching 1431 ± 38 d.nm for the 0.8 CEO-CHNPs/PEC film. This expansion in particle size is attributed to the hydrophobic nature of CEO, which promotes aggregation of the CHNPs. The zeta potential, a measure of electrostatic stability, decreased with increasing CEO concentration, indicating a reduction in electrostatic repulsion among the CHNPs. The negative zeta potential of -58 ± 1 mV of PEC FFS prepared at pH 7 is primarily due to the carboxyl groups of the carbohydrate (Esposito et al., 2016). These findings suggest that the incorporation of CEO into CHNPs leads to increased aggregation and reduced electrostatic repulsion due to its hydrophobic nature. It is worth noting that the size of the particles is quite homogeneous, being the PDI≤0.05.

Table 2. Z-average diameter (d.nm) and zeta potential (mV) of PEC films. The CHNPs: CEO ratios examined include 1:0.0, 1:0.1, 1:0.4, and 1:0.8.

FFS	Z-average diameter (d.nm)	%PDI	Zeta potential (mV)
PEC	867±4.0	0.32±0.03	-58±1
0.0 CEO-CHNPs/PEC	766 ±21	0.31±0.01	-57±2
0.1 CEO-CHNPs/PEC	929±17 [a,b]	0.42±0.03 [a,b]	-53±3
0.4 CEO-CHNPs/PEC	879 ±26 [b]	0.51±0.01 [a,b]	-55±1 [a]
0.8 CEO-CHNPs/PEC	1431±38 [a,b]	0.44±0.02 [a,b]	-50±3 [a,b]

The values that are significantly different compared to PEC FFS indicated by "a" ($p < 0.05$); the values indicated by "b" are significantly different ($p < 0.05$) from PEC unloaded with CEO. PDI, Polydispersity Index.

3.8.2. Mechanical characterization

The mechanical properties of PEC films were assessed with and without the incorporation of CHNPs (5 mg) and CEO. The addition of CHNPs into PEC films significantly enhanced their TS and YM, with TS values increasing from 2.00 ± 0.05 MPa to 6.00 ± 0.002 MPa and YM values increasing from 219.00 ± 60 MPa to 699.00 ± 50 MPa, respectively ($p<0.05$). These substantial increases in film strength and stiffness might be attributed to the interactions between CHNPs and PEC chains, which effectively crosslink and strengthen the polymer network which is likely attributable to the strengthened intermolecular interactions between biopolymer chains induced by nanoparticles. Comparable results were reported by Younis et al. 2019, who demonstrated that the addition of CH to PEC films resulted in a significantly enhanced TS of 6.49 MPa. Lorevice et al. 2016 demonstrated a similar trend, employing higher concentrations of PEC and CH while observing similar enhancements in film stiffness upon incorporating CHNPs. The authors attributed this improved stiffness to the complementary interactions between CH's amine groups and PEC carboxylic groups. When films are subjected to stress, they absorb energy through various mechanisms. Part of this energy is absorbed by stretching the bonds between polymer chains, enabling alignment without breakage. The addition of CHNPs to PEC matrices necessitates the alignment of more polymer chains, requiring more energy (dos Santos et al., 2023). Additionally, CHNPs are likely to disperse between adjacent chains, strengthening intermolecular interactions, reducing chain mobility, and consequently producing more resistant films. This mechanism could potentially explain the observed stiffness enhancement in this study (**Fig. 4**). The presence of CEO appeared to enhance the stiffness of the films, which is evident from the observation that the TS of the CEO-loaded films increased from 6.3 MPa for the unloaded film to 7.5 MPa for the 0.8 CEO-CHNPs/PEC film (**Fig. 4**). Conversely, the elongation at break (EB) decreased with increasing CEO content, indicating a reduction in film flexibility. The EB values ranged from 11% for the unloaded film to 4% for the 0.8 CEO-CHNPs/PEC film, suggesting that CEO-loaded films offer improved resistance. These findings align with previous studies, such as those of dos Santos et al. 2023, who investigated the effect of garlic oil-based CH nanocomposites on PEC films. The enhancement in mechanical properties can be attributed to the synergistic interactions between CEO, PEC, and CHNPs. CEO's aromatic compounds are known to interact with the hydroxyl groups on PEC molecules, forming hydrogen bonds that strengthen the polymer network. Additionally, the CEO's

hydrophobic nature can induce interactions with the CHNPs, further crosslinking the film matrix and enhancing its mechanical integrity.

The incorporation of CEO into CHNPs/PEC films not only improves their mechanical properties but also imparts antimicrobial and antioxidant properties which make CEO-CHNPs/PEC films a promising alternative to conventional synthetic packaging materials.

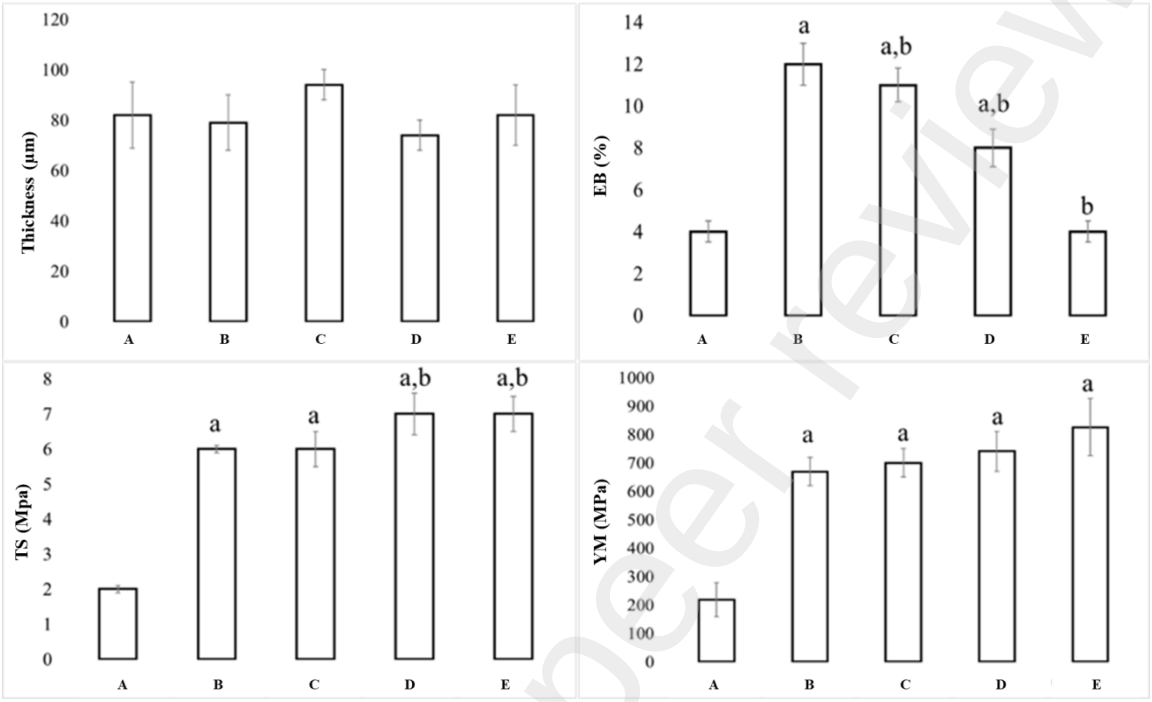

Fig. 4. Mechanical characterization (T, Thickness, TS; tensile strength; EB, elongation at break; YM, Young's modulus) of PEC-based films (A: PEC; B: 0.0 CEO-CHNPs/PEC; C: 0.1 CEO-CHNPs/PEC; D: 0.4 CEO-CHNPs/PEC and E: 0.8 CEO-CHNPs/PEC). The values that are significantly different compared to PEC unloaded with CH nanoparticles indicated by "a" ($p < 0.05$); the values indicated by "b" are significantly different ($p < 0.05$) from the films with CH nanoparticles- unloaded with CEO.

3.8.3. Morphological analysis

SEM images revealed distinct differences in surface morphology among unreinforced PEC films (**Fig. 5a**), PEC films loaded with CHNPs (**Fig. 5b**), and PEC films loaded with the highest amount of CEO (0.8 CEO-CHNPs/PEC) (**Fig. 5c**). The incorporation of CHNPs and CEO led to a rougher and more textured surface, with visible grooves and cracks, in contrast to the smoother surface of the unreinforced PEC film. The observed structural changes suggest that the addition of CHNPs and CEO influences the film formation process (Lei et al., 2016; Bravin et al., 2004). This aggregation, likely driven by the hydrophobic nature of CEO, could lead to the formation of a network of interconnected nanoparticles, potentially contributing to enhanced mechanical properties and water vapor barrier properties.

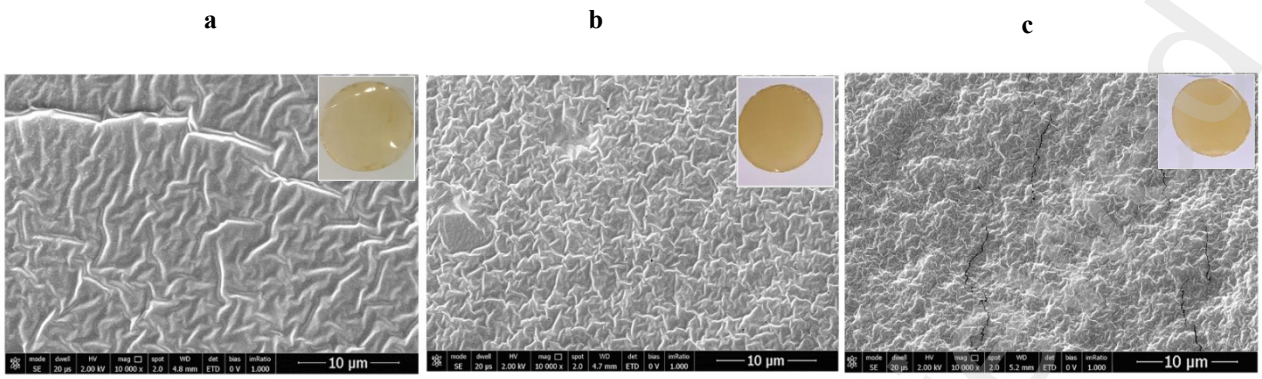

Fig. 5. Scanning electron microscopy analysis (SEM) of (a) PEC films;(b) PEC films containing CH nanoparticles (CHNPs); (c) PEC films with CEO (0.8 CEO-CHNPs/PEC) at magnification 10000 x.

3.8.4. Water vapor permeability (WVP)

Table 3 summarizes the effects of incorporating CEO-CHNPs at varying concentrations on the WVP of PEC-based films. The WVP of films containing CEO was initially higher compared to the control film (PEC alone, 3.9 ± 0.2 g mm m^{-2} d^{-1} kPa^{-1}). However, the WVP gradually decreased as the CEO concentration increased, indicating that CEO and CHNP-modified films significantly improved barrier properties compared to films without CEO. The CHNPs/PEC film exhibited a WVP value of 5.7 ± 0.2 g mm m^{-2} d^{-1} kPa^{-1}, and the lowest WVP was for PEC-based films with the lowest CEO, mainly for 0.4 CEO-CHNPs/PEC and 0.8 CEO-CHNPs/PEC. These values suggest the effectiveness of CEO, a mixture of hydrophobic compounds, such as allicin, in reducing WVP and permeance through the film. The observed result can be ascribed to the collaborative impact of the film matrix and the hydrophobic nature of the CEO. The uniform distribution of CEO within the polymer chains generates hydrophobic regions that effectively repel water molecules, diminishing interactions among hydrophilic groups. This, in turn, enhances the film barrier properties (Espitia et al., 2014; Martelli et al., 2013; Cazón et al., 2017; Aitboulahsen et al., 2020). Moreover, the high-methoxylated PEC contains fewer carboxyl groups, further reducing available hydrophilic sites for water interaction and permeation (Aitboulahsenet al., 2020). In conclusion, the incorporation of CEO-CHNPs into PEC- films significantly improved their barrier feature toward water. The synergistic interactions between CEO-CHNPs and PEC resulted in a more hydrophobic film matrix.

Table 3. Water vapor permeability (WVP) of PEC films. The CHNPs/CEO ratios examined include 1:0.0, 1:0.1, 1:0.4, and 1:0.8.

Films	Water vapor permeation [g mm m^{-2} d^{-1} kPa^{-1}]
PEC	3.9±0.2
0.0 CEO-CHNPs/PEC	5.7±0.2 [a]
0.1 CEO-CHNPs/PEC	5.1±0.1 [a]
0.4 CEO-CHNPs/PEC	4.4±0.2 [a,b]
0.8 CEO-CHNPs/PEC	4.4±0.4 [a,b]

The values that are significantly different compared to PEC unloaded with CH particles indicated by "a" ($p < 0.05$); the values indicated by "b" are significantly different ($p < 0.05$) from the films with CH particles unloaded with CEO.

3.8.5. Thermal properties

The results of DSC and TGA analysis on PEC-based films are reported in **Fig. 6**. As with CHNPs, PEC exhibits an exothermic peak associated with dehydration at 73°C. The addition of CHNPs at various CEO loadings to the PEC film does not affect the amount of water absorbed, as shown by the TGA thermogram, but decreases the entity of water-polymer interactions (Martelli et al., 2013), as deducible by the decrease of T_D to ~65 °C. Furthermore, the degradation temperature (~200°C) is only slightly affected by the addition of CEO-CHNPs, as well as the residue at 600°C, which is increased from 20% for PEC to 25% for the CEO-CHNPs/PEC.

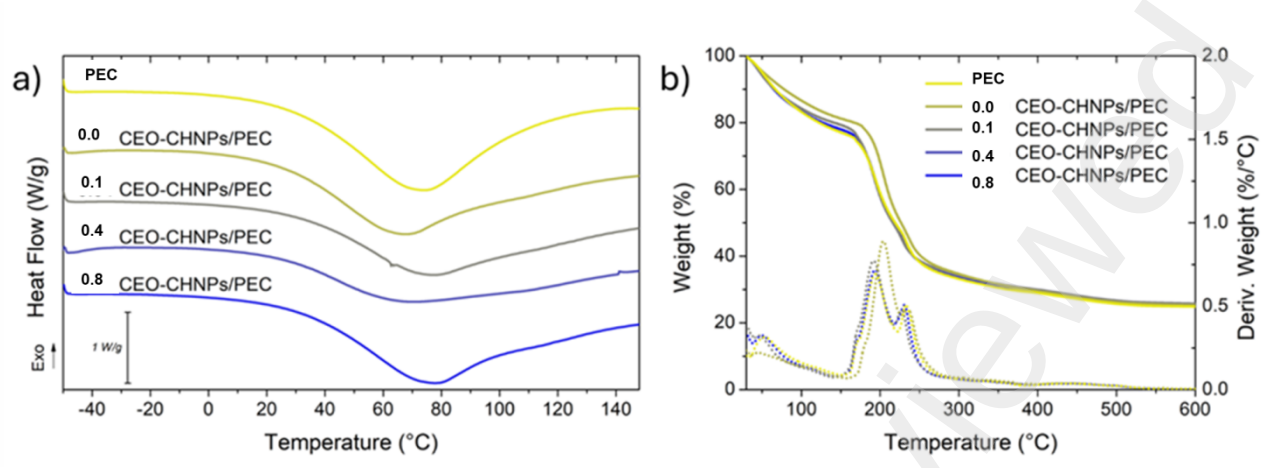

Fig. 6. (a) DSC and (b) TGA thermograms of PEC films and PEC films loaded with different CEO-loaded CHNPs.

4. Conclusion

In this study, we successfully encapsulated clove essential oil (CEO) within chitosan nanoparticles (CHNPs), achieving a maximum encapsulation efficiency of 16% and a loading capacity of 8%. The encapsulated CEO exhibited strong antioxidant activity against DPPH radicals (IC_{50} 2.7 ± 0.13 µg/mL), demonstrating its potential to protect food products from oxidative damage. These CEO-CHNPs were then incorporated into a Citrus pectin (PEC) matrix via polyelectrolyte complexation, yielding CEO-CHNPs/PEC films.

While the resulting films didn't show significantly enhanced barrier properties compared to pure pectin films, they did exhibit improved mechanical properties (increased stiffness) and enhanced thermal stability, which are desirable attributes for food packaging. Scanning electron microscopy revealed a porous microstructure, potentially influenced by the CHNPs.

Crucially, the developed CEO-CHNPs/PEC films demonstrated significant in vitro antibacterial activity against *Pectobacterium carotovorum* subsp. *carotovorum* (Pcc). Specifically, the CHNPs+0.16CEO formulation achieved total inhibition of Pcc growth at its highest concentration (0.3% w/v) and maintained strong inhibitory capacity even at its lowest concentration (0.003% w/v) after 2 days. This highlights the synergistic antimicrobial effect of CEO and CHNPs. Our findings confirm the feasibility of developing PEC-based films grafted with CEO-CHNPs as promising bioactive materials with both antioxidant and antimicrobial properties. Further research involving in-situ evaluation of their antioxidants and antimicrobial performance in real-world food systems is essential to validate their potential for practical post-harvest food preservation applications.

Author Contributions

Sondos Hejazi, Angela Marotta, Ana Aleksove: Writing – original draft, Validation, Investigation, Formal analysis, Data curation, Methodology. **C. Valeria L. Giosafatto**: Resources, Conceptualization, Visualization. **Sondos Hejazi, Angela Marotta, Ana Aleksove, Alessandro Polito**: Methodology, Investigation, Formal analysis. **C. Valeria L. Giosafatto**: Writing – review & editing, Validation, Supervision, Project administration, Conceptualization. **Valeria Scala:** Resources, Visualization. **Mohammed Sabbah, Valeria Scala, C. Valeria L. Giosafatto** Writing – review & editing.

Acknowledgements

The authors thank Mrs. Maria Fenderico, Dr. Antonella Giarra and Dr. Odile Francesca Restaino for their technical support in film preparation, microscopy analysis, and FTIR, respectively.

Funding

This research did not receive any specific grant from funding agencies in the public, commercial, or not-for-profit sectors.

Decleration

There are no conflicts to declare.

References

Abdalrazeq, M., Jaradat, N. M., Qadi, C. V. L. G., Dell'Olmo, E., Gaglione, R., Arciello, A., & Porta, R. (2021). Physicochemical and antimicrobial properties of whey protein-based films functionalized with Palestinian *Satureja capitata* essential oil. *Coatings*, *11*(11), 1364. https://doi.org/10.3390/coatings11111364

Aitboulahsen, M., El Galiou, O., Laglaoui, A., Bakkali, M., & Hassani Zerrouk, M. (2020). Effect of plasticizer type and essential oils on mechanical, physicochemical, and antimicrobial characteristics of gelatin, starch, and pectin-based films. *Journal of Food Processing and Preservation*, *44*(7), e14480. https://doi.org/10.1111/jfpp.14480

Ajun, W., Yan, S., Li, G., & Huili, L. (2009). Preparation of aspirin and probucol in combination loaded chitosan nanoparticles and in vitro release study. *Carbohydrate Polymers*, *75*(4), 566–574. https://doi.org/10.1016/j.carbpol.2008.08.019

Al-Asmar, A., Giosafatto, C. V. L., Sabbah, M., Sanchez, A., Villalonga Santana, R., & Mariniello, L. (2020). Effect of mesoporous silica nanoparticles on the physicochemical properties of pectin packaging material for strawberry wrapping. *Nanomaterials*, *10*(1), 52. https://doi.org/10.3390/nano10010052

Alkhader, E., Billa, N., & Roberts, C. J. (2017). Mucoadhesive chitosan-pectinate nanoparticles for the delivery of curcumin to the colon. *AAPS PharmSciTech*, *18*(4), 1009–1018. http://doi.org/10.1208/s12249-016-0623-y

Arciello, A., Panzella, L., Dell'Olmo, E., Abdalrazeq, M., Moccia, F., Agustin-Salazar, S., Napolitano, A., Mariniello, L., & Giosafatto, C. V. L. (2021). Development and characterization of antimicrobial and antioxidant whey protein-based films functionalized with Pecan (*Carya illinoinensis*) nut shell extract. *Food Packaging and Shelf Life*, *29*, 100710. https://doi.org/10.1016/j.fpsl.2021.100710

ASTM D882. (1997). *Standard test method for tensile properties of thin plastic sheeting*. ANSI Blog. Retrieved from https://www.astm.org/Standards/D882

ASTM F1249-13. (2013). *Standard test method for water vapor transmission rate through plastic film and sheeting using a modulated infrared sensor*.

Bravin, B., Peressini, D., & Sensidoni, A. (2004). Influence of emulsifier type and content on functional properties of polysaccharide lipid-based edible films. *Journal of Agricultural and Food Chemistry*, *52*(21), 6448–6455. https://pubs.acs.org/doi/full/10.1021/jf040065b

Cazón, P., Velazquez, G., Ramírez, J. A., & Vázquez, M. (2017). Polysaccharide-based films and coatings for food packaging: A review. *Food Hydrocolloids*, *68*, 136–148. https://doi.org/10.1016/j.foodhyd.2016.09.009

Chen, F., Shi, Z., Neoh, K., & Kang, E. (2009). Antioxidant and antibacterial activities of eugenol and carvacrol-grafted chitosan nanoparticles. *Biotechnology and Bioengineering*, *104*(1), 30–39.

Corrado, I., Abdalrazeq, M., Pezzella, C., Di Girolamo, R., Porta, R., Sannia, G., & Giosafatto, C. V. L. (2021). Design and characterization of poly (3-hydroxybutyrate-co-hydroxyhexanoate) nanoparticles and their grafting in whey protein-based nanocomposites. *Food Hydrocolloids*, *110*, 106167. https://doi.org/10.1016/j.foodhyd.2020.106167

De Moura, M. R., Aouada, F. A., & Mattoso, L. H. (2008). Preparation of chitosan nanoparticles using methacrylic acid. *Journal of Colloid and Interface Science*, *321*(2), 477–483. https://doi.org/10.1016/j.jcis.2008.02.006

dos Santos, V. S., Lorevice, M. V., Baccarin, G. S., da Costa, F. M., Fernandes, R. S., Aouada, F. A., & de Moura, M. R. (2023). Combining chitosan nanoparticles and garlic essential oil as additive fillers to produce pectin-based nanocomposite edible films. *Polymers*, *15*(10), 2244. https://doi.org/10.3390/polym15102244

Espitia, P. J. P., Du, W. X., Avena-Bustillos, R. J., Soares, N. D. F. F., & McHugh, T. H. (2014). Edible films from pectin: Physical-mechanical and antimicrobial properties-A review. *Food Hydrocolloids*, *35*, 287–296. https://doi.org/10.1016/j.foodhyd.2013.06.005

Esposito, E., Di Pierro, P., Regalado-Gonzales, C., Mariniello, L., Giosafatto, C. V. L., & Porta, R. (2016). Polyamines as new cationic plasticizers for pectin-based edible films. *Carbohydrate Polymers*, *153*, 22–228. https://doi.org/10.1016/j.carbpol.2016.07.087

Feyzioglu, G. C., & Tornuk, F. (2016). Development of chitosan nanoparticles loaded with summer savory (*Satureja hortensis* L.) essential oil for antimicrobial and antioxidant delivery applications. *LWT - Food Science and Technology*, *70*, 104–110. https://doi.org/10.1016/j.lwt.2016.02.037

Giosafatto, C. V. L., Di Pierro, P., Gunning, P., Mackie, A., Porta, R., & Mariniello, L. (2014). Characterization of Citrus pectin edible films containing transglutaminase-modified phaseolin. *Carbohydrate Polymers*, *106*, 200–208. https://doi.org/10.1016/j.carbpol.2014.02.015

Guan, W., Li, S., Yan, R., Tang, S., & Quan, C. (2007). Comparison of essential oils of clove buds extracted with supercritical carbon dioxide and other three traditional extraction methods. *Food Chemistry*, *101*, 1558–1564. https://doi.org/10.1016/j.foodchem.2006.04.009

Hasheminejad, N., Khodaiyan, F., & Safari, M. (2019). Improving the antifungal activity of clove essential oil encapsulated by chitosan nanoparticles. *Food Chemistry*, *275*, 113–122. https://doi.org/10.1016/j.foodchem.2018.09.085K. Chaieb, H. Hajlaoui, T. Zmantar, A. B. Kahla-Nakbi, □ Rouabhia, M., Mahdouani, K., & Bakhrouf, A. (2007). The chemical composition and biological activity of clove essential oil, *Eugenia caryophyllata* (*Syzigium aromaticum* L. Myrtaceae): a short review. *Phytotherapy Research*, *21*, 501–506. https://doi.org/10.1002/ptr.2124

He, C., Hu, Y., Yin, L., Tang, C., & Yin, C. (2010). Effects of particle size and surface charge on cellular uptake and biodistribution of polymeric nanoparticles. *Biomaterials*, *31*(14), 3657–3666. https://doi.org/10.1016/j.biomaterials.2010.01.065

Hejazi, S., Carpentieri, A., Marotta, A., Restaino, O. F., Solimeno, I., Zannini, D., & Giosafatto, C. V. L. (2024). Chitosan/poly-γ-glutamic acid crosslinked hydrogels: Characterization and application as bio-glues. *International Journal of Biological Macromolecules*, *277*, 133653. https://doi.org/10.1016/j.ijbiomac.2024.133653

Hejazi, S., Restaino, O. F., Sabbah, M., Zannini, D., Di Girolamo, R., Marotta, A., & Giosafatto, C. V. L. (2023). Physicochemical characterization of chitosan/poly-γ-glutamic acid glass-like materials. *International Journal of Molecular Sciences*, *24*(15), 12495. https://doi.org/10.3390/ijms241512495

Hosseini, S. F., Zandi, M., Rezaei, M., & Farahmandghavi, F. (2013). Two-step method for encapsulation of oregano essential oil in chitosan nanoparticles: Preparation, characterization and in vitro release study. *Carbohydrate Polymers*, *95*, 50–56. https://doi.org/10.1016/j.carbpol.2013.02.031

Hu, Q., & Luo, Y. (2016). Polyphenol-chitosan conjugates: Synthesis, characterization, and applications. *Carbohydrate Polymers*, *151*, 624–639. https://doi.org/10.1016/j.carbpol.2016.05.109

Iijima, M., Nakamura, K., Hatakeyama, T., & Hatakeyama, H. (2000). Phase transition of pectin with sorbed water. *Carbohydrate Polymers*, *41*, 101–106. https://doi.org/10.1016/S0144-8617(99)00116-2

Jamil, B., Abbasi, R., Abbasi, S., Imran, M., Khan, S. U., Ihsan, A., & Ahmad, S. (2016). Encapsulation of cardamom essential oil in chitosan nano-composites: In-vitro efficacy on antibiotic-resistant bacterial

pathogens and cytotoxicity studies. *Frontiers in Microbiology*, *7*, Article 1580. https://doi.org/10.3389/fmicb.2016.01580

Jílková, B., Víchová, J., Holková, L., Pluháčková, H., Michutová, M., & Kmoch, M. (2024). Laboratory efficacy of essential oils against *Pectobacterium carotovorum* subsp. *carotovorum* and *Pectobacterium atrosepticum* causing soft rot of potato tubers. *Potato Research*. https://doi.org/10.1007/s11540-024-09743-y

Joshi, J. R., Khazanov, N., Senderowitz, H., Burdman, S., Lipsky, A., & Yedidia, I. (2016). Plant phenolic volatiles inhibit quorum sensing in pectobacteria and reduce their virulence by potential binding to ExpI and ExpR proteins. *Scientific Reports*, *6*, Article 38126. https://doi.org/10.1038/srep38126

Katouzian, I., & Jafari, S. (2016). Nano-encapsulation as a promising approach for targeted delivery and controlled release of vitamins. *Trends in Food Science & Technology*, *53*, 34–48. https://doi.org/10.1016/j.tifs.2016.05.002

Keawchaoon, L., & Yoksan, R. (2011). Preparation, characterization and in vitro release study of carvacrol-loaded chitosan nanoparticles. *Colloids and Surfaces B: Biointerfaces*, *84*(1), 163–171. https://doi.org/10.1016/j.colsurfb.2010.12.031

Khajeh, M., Yamini, Y., & Sefidkon, F. (2004). Comparison of essential oil composition of *Carum copticum* obtained by supercritical carbon dioxide extraction and hydrodistillation methods. *Food Chemistry*, *86*(4), 587–591. https://doi.org/10.1016/j.foodchem.2003.09.041

Kiki, M. J. (2023). In vitro antiviral potential, antioxidant, and chemical composition of clove (*Syzygium aromaticum*) essential oil. *Molecules*, *28*(6), 2421. https://doi.org/10.3390/molecules28062421

Lei, Y., Wu, H., Jiao, C., Jiang, Y., Liu, R., Xiao, D., & Li, S. (2019). Investigation of the structural and physical properties, antioxidant and antimicrobial activity of pectin-konjac glucomannan composite edible films incorporated with tea polyphenol. *Food Hydrocolloids*, *94*, 128–135. https://doi.org/10.1016/j.foodhyd.2019.03.011

Lesjak, M., Beara, I., Simin, N., Pintać, D., Majkić, T., Bekvalac, K., Orčić, D., Balog, M., & Mimica-Dukić, N. (2018). Antioxidant and anti-inflammatory activities of quercetin and its derivatives. *Journal of Functional Foods*, *40*, 68–75. https://doi.org/10.1016/j.jff.2017.10.047

Lim, J.-A., Jee, S., Lee, D. H., Roh, E., Jung, K., Oh, C., & Heu, S. (2013). Biocontrol of *Pectobacterium carotovorum* subsp. *carotovorum* using bacteriophage PP1. *Journal of Microbiology and Biotechnology*, *23*(7), 1013–1020. https://doi.org/10.4014/jmb.1304.04001

Lorevice, M. V., Otoni, C. G., de Moura, M. R., & Mattoso, L. H. C. (2016). Chitosan nanoparticles on the improvement of thermal, barrier, and mechanical properties of high-and low-methyl pectin films. *Food Hydrocolloids*, *52*, 732–740. https://doi.org/10.1016/j.foodhyd.2015.08.003

Martelli, M. R., Barros, T. T., de Moura, M. R., Mattoso, L. H., & Assis, O. B. (2013). Effect of chitosan nanoparticles and pectin content on mechanical properties and water vapor permeability of banana puree films. *Journal of Food Science*, *78*(1), 98–104. https://doi.org/10.1111/j.1750-3841.2012.03006.x

Mirpoor, S. F., Giosafatto, C. V. L., Mariniello, L., D'Agostino, A., D'Agostino, M., Cammarota, M., Schiraldi, C., & Porta, R. (2022). Argan (*Argania spinosa* L.) seed oil cake as a potential source of protein-based film matrix for pharmaco-cosmetic applications. *International Journal of Molecular Sciences*, *23*(15), 8478. https://doi.org/10.3390/ijms23158478

Mirpoor, S. F., Zannini, D., Santagata, G., & Giosafatto, C. V. L. (2024). Cardoon seed oil cake proteins as substrate for microbial transglutaminase: Their application as matrix for bio-based packaging to extend the shelf-life of peanuts. *Food Hydrocolloids*, *147*, 109339. https://doi.org/10.1016/j.foodhyd.2023.109339

Radzig, M., Nadtochenko, V., Koksharova, O., Kiwi, J., Lipasova, V., & Khmel, I. (2013). Antibacterial effects of silver nanoparticles on gram-negative bacteria: Influence on the growth and biofilms formation, mechanisms of action. *Colloids and Surfaces B: Biointerfaces*, *102*, 300–306.

Rahaiee, S., Shojaosadati, A., Hashemi, M., Moini, S., & Razavi, S. H. (2015). Improvement of crocin stability by biodegradable nanoparticles of chitosan-alginate. *International Journal of Biological Macromolecules*, *79*, 423–432. https://doi.org/10.1016/j.ijbiomac.2015.04.041

Reverchon, E. (1997). Supercritical fluid extraction and fractionation of essential oils and related products. *The Journal of Supercritical Fluids*, *10*(1), 1–37. https://doi.org/10.1016/S0896-8446(97)00014-4

Rodríguez, J., Martín, M. J., Ruiz, M. A., & Clares, B. (2016). Current encapsulation strategies for bioactive oils: From alimentary to pharmaceutical perspectives. *Food Research International*, *83*, 41–59. https://doi.org/10.1016/j.foodres.2016.01.032

Russo, E., Gaglianone, N., Baldassari, S., Parodi, B., Cafaggi, S., Zibana, C., & Del Gaudio, M. (2014). Preparation, characterization and in vitro antiviral activity evaluation of foscarnet-chitosan nanoparticles. *Colloids and Surfaces B: Biointerfaces*, *118*, 117–125. https://doi.org/10.1016/j.colsurfb.2014.03.037

Sabbah, M., Al-Asmar, A., Younis, D., Al-Rimawi, F., Famiglietti, M., & Mariniello, L. (2023). Production and characterization of active pectin films with olive or guava leaf extract used as soluble sachets for chicken stock powder. *Coatings*, *13*(7), Article 1253.

Sanpui, P., Murugadoss, A., Durga, P., Sankar, S., & Chattopadhyay, A. (2008). The antibacterial properties of a novel chitosan-Ag-nanoparticle composite. *International Journal of Food Microbiology*, *124*(2), 142–146.

Sebaaly, C., Jraij, A., Fessi, H., Charcosset, C., & Greige-Gerges, H. (2015). Preparation and characterization of clove essential oil-loaded liposomes. *Food Chemistry*, *178*, 52–62. https://doi.org/10.1016/j.foodchem.2015.01.067

Selles, S. M. A., Kouidri, M., Belhamiti, B. T., & Amrane, A. A. (2020). Chemical composition, in-vitro antibacterial and antioxidant activities of *Syzygium aromaticum* essential oil. *Journal of Food Measurement and Characterization*, *14*, 2352–2358. https://doi.org/10.1007/s11694-020-00482-5

Sotelo-Boyás, M. E., Correa-Pacheco, Z. N., Bautista-Baños, S., & Corona-Rangel, M. L. (2017). Physicochemical characterization of chitosan nanoparticles and nanocapsules incorporated with lime essential oil and their antibacterial activity against food-borne pathogens. *LWT - Food Science and Technology*, *77*, 15–20. https://doi.org/10.1016/j.lwt.2016.11.022

Sotelo-Boyás, M. E., Valverde-Aguilar, G., Plascencia-Jatomea, M., Correa-Pacheco, Z. N., Jiménez-Aparicio, A., Solorza-Feria, J., Barrera-Necha, L., & Bautista-Baños, S. (2015). Characterization of chitosan nanoparticles added with essential oils: In vitro effect on *Pectobacterium carotovorum*. *Revista Mexicana de Ingeniería Química*, *14*(3), 589–599.

Woranuch, S., & Yoksan, R. (2013). Eugenol-loaded chitosan nanoparticles: I. Thermal stability improvement of eugenol through encapsulation. *Carbohydrate Polymers*, *96*, 578–585. https://doi.org/10.1016/j.carbpol.2012.08.117

Yoksan, R., Jirawutthiwongchai, J., & Arpo, K. (2010). Encapsulation of ascorbyl palmitate in chitosan nanoparticles by oil-in-water emulsion and ionic gelation processes. *Colloids and Surfaces B: Biointerfaces*, *76*(1), 292–297. https://doi.org/10.1016/j.colsurfb.2009.11.007

Younes, I., & Rinaudo, M. (2015). Chitin and chitosan preparation from marine sources. Structure, properties and applications. *Marine Drugs*, *13*(3), 1133–1174. https://doi.org/10.3390/md13031133

Younis, H. G., & Zhao, G. (2019). Physicochemical properties of the edible films from the blends of high methoxyl apple pectin and chitosan. *International Journal of Biological Macromolecules*, *131*, 1057–1066. https://doi.org/10.1016/j.ijbiomac.2019.03.096

Zhang, J., Tian, Y., Wang, J., Ma, L., Liu, L., Islam, R., Qi, Y., Li, J., & Shen, T. (2023). Inhibitory effect and possible mechanism of oregano and clove essential oils against *Pectobacterium carotovorum* subsp. *carotovorum* as onion soft rot in storage. *Postharvest Biology and Technology*, *196*, 112164. https://doi.org/10.1016/j.postharvbio.2023.112164